BIOCHEMISTRY
including biophysical chemistry & molecular biology

ARTICLE

pubs.acs.org/biochemistry

Phosphatidylinositol 4,5-Bisphosphate Alters Synaptotagmin 1 Membrane Docking and Drives Opposing Bilayers Closer Together

Weiwei Kuo, Dawn Z. Herrick, and David S. Cafiso*

Department of Chemistry and Center for Membrane Biology, University of Virginia, Charlottesville, Virginia 22904-4319, United States

ABSTRACT: Synaptotagmin 1 (syt1) is a synaptic vesicle-anchored membrane protein that acts as the calcium sensor for the synchronous component of neuronal exocytosis. Using site-directed spin labeling, the position and membrane interactions of a fragment of syt1 containing its two C2 domains (syt1C2AB) were assessed in bilayers containing phosphatidylcholine (PC), phosphatidylserine (PS), and phosphatidylinositol 4,5-bisphosphate (PIP_2). Addition of 1 mol % PIP_2 to a lipid mixture of PC and PS results in a deeper membrane penetration of the C2A domain and alters the orientation of the C2B domain so that the polybasic face of C2B comes into the proximity of the bilayer interface. The C2B domain is found to contact the membrane interface in two regions, the Ca^{2+}-binding loops and a region opposite the Ca^{2+}-binding loops. This suggests that syt1C2AB is configured to bridge two bilayers and is consistent with a model generated previously for syt1C2AB bound to membranes of PC and PS. Point-to-plane depth restraints, obtained by progressive power saturation, and interdomain distance restraints, obtained by double electron−electron resonance, were obtained in the presence of PIP_2 and used in a simulated annealing routine to dock syt1C2AB to two membrane interfaces. The results yield an average structure different from what is found in the absence of PIP_2 and indicate that bilayer−bilayer spacing is decreased in the presence of PIP_2. The results indicate that PIP_2, which is necessary for bilayer fusion, alters C2 domain orientation, enhances syt1−membrane electrostatic interactions, and acts to drive vesicle and cytoplasmic membrane surfaces closer together.

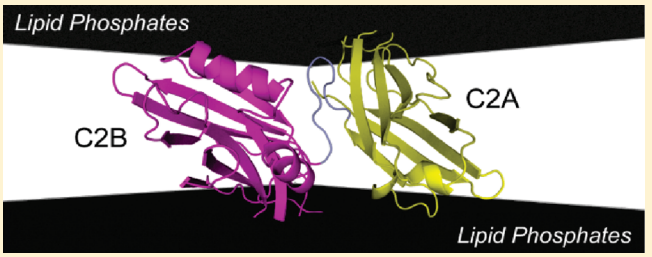

In the central nervous system, neurotransmitter release is mediated by a tightly regulated Ca^{2+}-triggered membrane fusion event. The SNARE (soluble *N*-ethylmaleimide-sensitive factor attachment protein receptor) proteins assemble into a stable four-helix bundle and make up the central protein machinery that drives this fusion process.[1−5] The prevailing model for SNARE activity, sometimes termed the SNARE hypothesis, proposes that the assembly and folding of the SNARE proteins (syntaxin, SNAP-25, and synaptobrevin) in an N-terminal to C-terminal direction drive fusion of the vesicle and plasma membranes.[5] However, a number of other proteins regulate and are critical in this process, including CAPS, Munc18, complexin, and synaptotagmin 1.[6,7]

In the neuronal system, there is strong evidence that synaptotagmin 1 (syt1) acts as the Ca^{2+} sensor for the synchronous component of exocytosis. A transmembrane helical segment anchors syt1 to the synaptic vesicle, and it contains two cytoplasmic C2 domains, termed C2A and C2B, that are C-terminal to the membrane anchor (Figure 1). Both C2A and C2B bind Ca^{2+} and penetrate membranes containing negatively charged phospholipids in a Ca^{2+}-dependent manner.[8−12] The C2B domain has a second weaker mode of binding to both PC/PIP_2 and PC/PS bilayers that is Ca^{2+}-independent.[8,13] In addition to these membrane interactions, syt1 is also reported to interact with the SNARE complex;[1,2,4,14] however, the structure of syt1 when associated with the SNARE complex does not appear to be well-defined, and syt1 may sample multiple conformational substates when bound to SNAREs.[15−17]

At present, the mechanism by which syt1 regulates membrane fusion has not been determined. Synaptotagmin 1 has been reported to alter membrane curvature, and this activity might promote the formation of a fusion stalk.[18,19] The interactions of syt1 with the SNAREs could assist in driving SNARE assembly, or these interactions might promote SNARE folding from an intermediate metastable state.[20] Synaptotagmin 1 also has the ability to bridge bilayers. Several studies indicate that syt1 aggregates vesicles in a Ca^{2+}-dependent manner,[21,22] and depth and interdomain distance restraints obtained by site-directed spin labeling (SDSL) can be satisfied only if C2A and C2B align in an antiparallel manner so that C2A and C2B bind to opposing bilayers.[23]

Electrostatic interactions play an important role in the membrane binding activity of syt1. For example, the Ca^{2+}-dependent membrane attachment of the syt1 C2A domain is mediated by Coulombic interactions with the negatively charged membrane surface, which are switched on when Ca^{2+} binds C2A.[24] Coulombic interactions are also important in the membrane interactions of C2B, and the Ca^{2+}-independent binding of C2B to membranes is mediated by a highly charged polybasic face on C2B.[13] Two conserved arginine residues on C2B, which are located opposite the Ca^{2+}-binding face, appear to be critical for

Received: January 12, 2011
Revised: February 22, 2011
Published: February 24, 2011

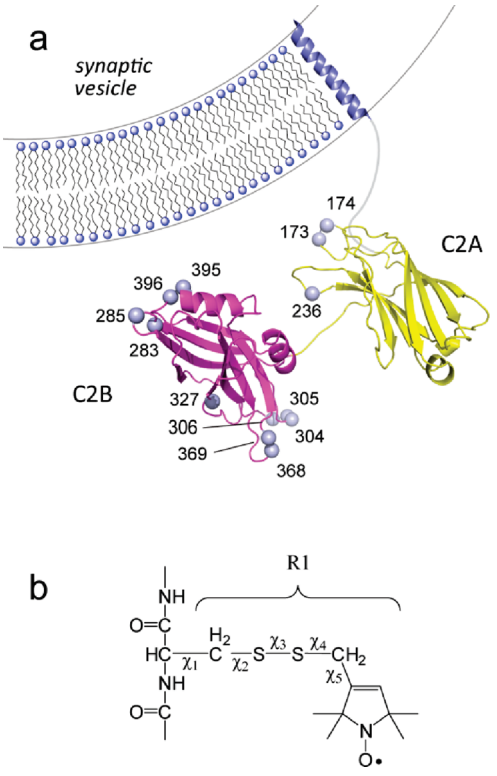

Figure 1. (a) Synaptotagmin 1 is a vesicle-anchored protein containing two C2 domains [C2A (yellow) and C2B (magenta)]. The membrane-bound conformation of a soluble fragment of synaptotagmin 1 containing its two C2 domains, syt1C2AB, was determined in the presence of 1 mol % PIP_2. The spheres represent Cα atoms for positions that have been derivatized with the spin-labeled side chain R1. (b) Spin-labeled side chain R1 that is obtained via derivatization of a cysteine residue with a methanethiosulfonate label.

membrane fusion and the ability of C2B to aggregate lipid vesicles[25] and for the attachment of this region to the membrane interface.[23]

The phosphorylated inositol lipid phosphatidylinositol 4,5-bisphosphate [PI(4,5)P_2 or PIP_2] is an essential signaling lipid that is required for membrane fusion.[26,27] While PIP_2 levels average ~1 mol % in the plasma membrane,[28] PIP_2 can reach levels of up to 6 mol % at sites of active exocytosis in PC12 cells.[29] Because PIP_2 has a valence of approximately $z = -4$ at neutral pH,[30] PIP_2 likely makes a major contribution to the membrane charge density during exocytosis. Moreover, because of the high valence of this lipid, the discreteness of charge effects become important and electrostatic interactions with proteins are enhanced relative to equivalent charge densities of monovalent lipids such as PS.[30] As a result, relatively low levels of PIP_2 might be expected to have significant effects on the interactions made by the syt1 C2 domains with bilayers. There are reports that PIP_2 accelerates the membrane binding of the C2B domain and alters the membrane binding mode of C2B.[8,12]

In this study, we made use of SDSL to examine the effect of low levels of PIP_2 on the conformation of a fragment of syt1 containing its two C2 domains (syt1C2AB) when membrane-associated in the presence of Ca^{2+}. A number of sites in syt1C2AB were derivatized with the spin-labeled side chain R1 (see Figure 1b), and a combination of continuous wave and pulse EPR was used to obtain bilayer depth restraints and interdomain distance restraints when syt1C2AB is bound to PC/PS/PIP_2 bilayers. The results of a simulated annealing procedure using these restraints can be satisfied only if syt1C2AB bridges two bilayers, which was seen previously for membranes containing PC and PS.[23] However, the addition of just 1 mol % PIP_2 to a PC/PS mixture enhances the electrostatic interaction between the C2B polybasic face and the membrane surface, producing a change in the orientation of the C2B domain. The Ca^{2+}-binding face of C2A penetrates more deeply into the lipid interface, and the region opposite the Ca^{2+}-binding loops of C2B maintains contact with the bilayer interface. As a result, the model indicates that low levels of PIP_2 help drive opposing bilayers that are bridged by syt1 closer together. The implications of this PIP_2-mediated structural change in syt1 for membrane fusion are discussed.

MATERIALS AND METHODS

Mutagenesis, Protein Expression, and Purification. For the cytosolic domain of rat syt1 C2A (residues 96−265), C2B (residues 249−421), and C2AB (residues 96−421) cysteine mutants, DNA modification, protein expression, and purification were conducted as previously described.[13,23] In brief, individual cysteine residues were introduced at positions in the tandem C2A, C2B, and C2AB domains using the QuickChange Site-Directed Mutagenesis Kit (Stratagene, La Jolla, CA) or two-step polymerase chain reaction (PCR), following published protocols.[31] All cysteine substitutions were confirmed by DNA sequencing. The mutants were expressed and purified with GST affinity and ion-exchange chromatography. For C2B and C2AB, the purity of protein was confirmed with a UV spectrum to have maximal absorption at 278 nm. The pure protein was treated with EDTA to ensure it was free of Ca^{2+}, lyophilized in NH_4HCO_3, and kept at −20 °C until it was labeled. Single-cysteine residues 256 of C2A, 415 of C2B, and 269 of C2AB were used for vesicle sedimentation measurements; C2AB single cysteine mutants (at positions 173, 174, 236, 283, 285, 304−306, 327, 368, 369, 395, and 396) and double cysteine mutants (at positions 199 and 304, 199 and 332, 213 and 283, and 213 and 353) were used for EPR experiments.

Liposome Preparations. 1-Palmitoyl-2-oleoyl-*sn*-glycero-3-phosphatidylcholine (POPC), 1-palmitoyl-2-oleoyl-*sn*-glycero-3-phosphatidylserine (POPS), and L-α-phosphatidylinositol 4,5-bisphosphate (ammonium salt) (PIP_2) (Avanti Polar Lipids, Alabaster, AL) were used to prepare large unilamellar vesicles (74:25:1 or 70:25:5 POPC:POPS:PIP_2 molar ratio) with the extrusion method. To produce evenly distributed PIP_2 membranes, we took extra caution when preparing PIP_2-containing vesicles.[32] Adequate amounts of POPC, POPS, and PIP_2 in chloroform were mixed in a 50 mL round-bottom flask, which was attached to a rotary evaporator and immersed in a 30−35 °C water bath. The flask was rotated without vacuum for 5 min, and then a maximal vacuum was slowly applied to dry the lipid mixture. Additional chloroform could be added, and the drying process could be repeated to yield an evenly coated lipid film on the flask. The resulting lipid film was vacuum desiccated overnight, rehydrated in either sucrose buffer [176 mM sucrose and 1 mM MOPS (pH 7.0)] or EPR buffer [100 mM NaCl and 20 mM HEPES (pH 7.4)], cycled through five freeze−thaw cycles, and extruded through 0.1 μm polycarbonate filters using a hand-held Mini-Extruder (Avanti Polar Lipids, Alabaster, AL).

Fluorescence and Spin Labeling of syt1 C2 Domains. Lyophilized syt1 C2A, C2B, and C2AB domains were first brought up in EPR buffer or salt buffer [100 mM KCl and 20 mM MOPS (pH 7.0)], then spin-labeled using methanethiosulfoate (MTSL) (Toronto Research Chemicals, Toronto, ON) at a 1:3:30 protein:DTT:MTSL molar ratio, or fluorescence-labeled using Bodipy-FL C1-IA (Invitrogen, Carlsbad, CA) at a 1:8:10 protein:TCEP:Bodipy-FL molar ratio. The excess spin-labels and fluorescence labels were removed with a HiPrep desalting column (GE Healthcare, Piscataway, NJ). The labeled protein was concentrated to 20−300 μM using an Amicon micro concentrator (Millipore, Billerica, MA). Spin-labeled protein was stored in EPR buffer where it was in a Ca^{2+}-free state. For sedimentation assays under Ca^{2+}-free conditions, additional 1 mM EGTA was added to the protein samples. Additional $CaCl_2$ (final concentration of 1 mM) was added to the samples for the Ca^{2+} condition in the EPR study.

EPR Spectroscopy. EPR spectra were recorded at room temperature using a Varian E-line Century series spectrometer fitted with a microwave preamplifier and an X-band loop gap resonator (Medical Advances, Milwaukee, WI); 20−300 μM aqueous syt1 protein was mixed with POPC/POPS/PIP_2 (75:25:1) LUVs (25 mM total lipid) for membrane-associated spectra. Continuous wave (CW) power saturation experiments were performed using a Bruker EMX spectrometer with a dielectric resonator, and results were used to calculate a depth parameter, Φ, based upon the saturation behavior of the samples containing oxygen and 10 mM Ni(II)EDDA. $\Delta P_{1/2}$ values of Ni(II)EDDA was scaled to an effective concentration of 20 mM. Distances were calculated on the basis of eq 1 obtained previously describing the correlation of distance (x) and Φ values.[33]

$$\Phi = 3.4 \tanh[0.11(x - 8.56)] + 1.1 \quad (1)$$

Depth measurements using a collision gradient approach may vary with lipid composition, and the validity of eq 1 for POPC/POPS mixtures containing low levels of PIP_2 was tested by measuring Φ for spin-labeled lipids in the presence and absence of 1 mol % PIP_2. Incorporation of PIP_2 at this low level in POPC/POPS mixtures had no measurable effect on Φ and did not alter the oxygen or Ni(II)EDDA $\Delta P_{1/2}$ value.

Pulse EPR measurements and sample preparation were described previously.[23] In brief, a 25−30 μL doubly labeled protein sample with 1 mM Ca^{2+}, POPC/POPS/PIP_2 (74:25:1) vesicles, and 10−20% (v/v) glycerol was loaded into quartz capillaries. Samples were flash-frozen in a dry ice/2-propanol bath, and the data were recorded at 80 K on a Bruker Elexsys E580 spectrometer fitted with an ER4118X-MS3 split-ring resonator (Bruker Biospin, Billerica, MA). The phase-corrected dipolar evolution data were processed assuming a three-dimensional background and Fourier transformed, and the distance distributions were obtained with a Gaussian fit using DeerAnalysis2009.

Vesicle Sedimentation Assay. Vesicle sedimentation assays were conducted as described previously,[34] and free protein concentrations were determined from the fluorescence of a Bodipy-labeled protein or the intrinsic fluorescence of the native protein. Here, experiments were conducted with 0.1−0.5 μM Bodipy-labeled C2A protein, ∼10 nM C2B, and ∼1 μM unlabeled C2AB 269. Additional 1 mM $CaCl_2$ or 1 mM EGTA was added under conditions with and without Ca^{2+} with sucrose-loaded LUVs at lipid concentrations ranging from 1 μM to 12 mM. The final lipid concentration was confirmed with a phosphate assay.[35] The emission spectrum taken with the FluoroMax-3 fluorimeter (Jobin Yvon, Edison, NJ) with excitation at 480 nm and emission at 510 nm was measured for the binding calculation of C2A and C2AB; the tryptophan fluorescence of C2AB was recorded with excitation at 290 nm and emission at 342 nm. At least three sets of measurements were taken for each lipid concentration and used to determine a molar partition coefficient, K, which is defined as

$$\frac{[P]_m}{[L]} = K[P] \quad (2)$$

where [P] is the concentration of protein in the bulk aqueous phase, $[P]_m$ is the molar concentration of protein bound to the membrane, and [L] is the molar concentration of accessible lipid. Here, the protein concentrations are dilute ([lipid] ≫ [protein]), so the fraction of protein bound, f_b, will be given by

$$f_b = \frac{K[L]}{1 + K[L]} \quad (3)$$

The data were fit to eq 2 using OriginPro version 7.5 to yield a value of K, the reciprocal molar partition coefficient in units of inverse molar.

Modeling the Membrane Docking of syt1C2AB. Models for the membrane-bound structure of syt1C2AB were generated in a manner similar to that described previously.[23] Briefly, the spin-labeled side chain R1 was appended to the structure at appropriate locations, and the first two dihedral angles for the side chain, χ_1 and χ_2, were set to −60°. A simulated annealing routine was performed without any experimental restraints to allow other side chain atoms to find reasonable conformations. The result of this procedure was the starting structure for the membrane docking simulation during which the entire spin-label side chain conformations were fixed in addition to the backbone atoms of the two C2 domains. The distances from the R1 side chains (at positions of 173, 174, 236, 283, 285, 304−306, 327, 368, 369, 395, and 396 of C2AB) to the membrane surface were calculated from the experimentally determined Φ values as described previously.[13] Simulated annealing was performed with restraints based on power saturation (distances to plane) and DEER (interdomain distances of residues 199−304, 199−332, 213−283, and 213−353). Structures were visualized and analyzed with PyMOL (DeLano Scientific LLC, Palo Alto, CA). Average angles and distances were measured with Discovery Studio Visualizer version 2.5 (Accelrys, San Diego, CA).

Electrostatic Calculations of the syt1 C2B Domain. The Adaptive Poisson−Boltzmann Solver (APBS) plug-in[36] within PyMOL was used to calculate electrostatic potential maps on the NMR solution structure of C2B (Protein Data Bank entry 1K5W).[37] The Ca^{2+}-bound C2B electrostatic profile was determined with the radius of the two Ca^{2+} ions set to 1.06 Å.[38] Protein and solvent dielectric constants were set to 2 and 78, respectively. A graphical representation of the calculated electrostatic potential isocontours in 150 mM monovalent ions at 1kT/e (approximately 25 mV) was displayed using PyMOL.

RESULTS

PI(4,5)P_2 at 1% Alters the Orientation of and Depth of Penetration of syt1C2AB. The spin-labeled side chain R1 was incorporated into the soluble fragment of syt1 containing its two C2 domains (syt1C2AB) at 13 different positions via derivatization of a single cysteine mutant with the MTSL reagent

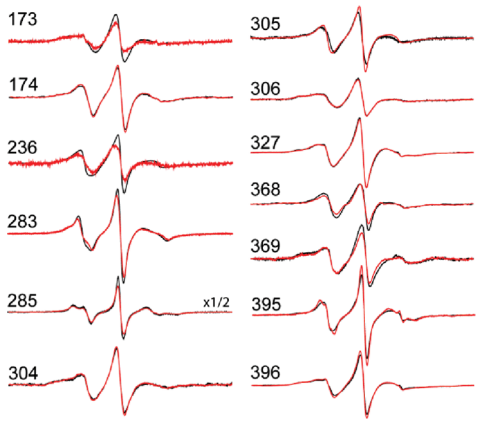

Figure 2. X-Band EPR spectra obtained from single R1 substitutions in syt1C2AB in the presence of Ca^{2+}. Spectra recorded in the presence of POPC/POPS (3:1) lipid vesicles are colored black, and spectra recorded in the presence of POPC/POPS/PIP_2 (74:25:1) lipid vesicles are colored red. Spectra are normalized against the total spin number so that the amplitudes provide an approximate measure of the motional averaging of the R1 side chain. All the spectra are 100 G scans.

Table 1. Depth Parameters, Φ, for Spin-Labeled Sites on syt1C2AB Associated with POPC/POPS (3:1) or POPC/POPS/PIP_2 (74:25:1) Bilayers in the Presence of Calcium[a]

labeled site	Φ (PC/PS)	Φ (PC/PS/PIP_2)	distance (Å)	range (Å)
M173R1	0.8 ± 0.3	1.2 ± 0.3	8.8	8.0 < *x* < 9.6
G174R1	0.6 ± 0.1	1.8 ± 0.2	10.5	9.9 < *x* < 11.0
K236R1	−0.3 ± 0.2	1.2 ± 0.2	8.8	8.2 < *x* < 9.3
V283R1	−1.9 ± 0.1	−2.2 ± 0.1	−10.6	−35.0 < *x* < −7.3
T285R1	−1.4 ± 0.1	−1.5 ± 0.1	−0.6	−1.3 < *x* < 0.0
V304R1	−0.4 ± 0.2	0.4 ± 0.3	6.7	5.8 < *x* < 7.5
G305R1	0.8 ± 0.2	−1.1 ± 0.1	1.6	1.1 < *x* < 2.0
G306R1	0.3 ± 0.3	0.2 ± 0.1	6.1	5.8 < *x* < 6.4
K327R1	−2.2 ± 0.2	−1.7 ± 0.1	−2.1	−3.0 < *x* < −1.3
G368R1	0.6 ± 0.1	−0.9 ± 0.1	2.4	0.6 < *x* < 3.9
K369R1	−1.2 ± 0.2	0.5 ± 0.2	6.9	6.4 < *x* < 7.5
A395R1	−1.0 ± 0.1	−1.9 ± 0.1	−4.0	−5.4 < *x* < −3.0
N396R1	−2.1 ± 0.1	−1.4 ± 0.1	0.0	−0.6 < *x* < 0.6

[a] The distances and range were calculated for PIP_2-containing bilayers. Depth parameters were obtained by progressive power saturation of the EPR spectra and were used to estimate depths as described in Materials and Methods. The range was determined by uncertainty in the measured values of Φ and eq 1.

(Figure 1). Most of these positions were chosen for labeling because the R1 label was seen previously to penetrate POPC/POPS bilayers or because the EPR spectra of R1 exhibited changes upon membrane association. Shown in Figure 2 are the X-band EPR spectra of these single R1 mutants when fully associated with either POPC/POPS (3:1) or POPC/POPS/PIP_2 (74:25:1) vesicles in the presence of Ca^{2+} (black or red traces, respectively). The line shapes at each site are a reflection of the local structure at each labeled position as well as the penetration of the label into the membrane hydrocarbon.[10] For most sites, no significant differences in the EPR spectra are seen, indicating that the label motion at these sites is unchanged by the presence of 1 mol % PIP_2. However, there are small but significant differences in the spectra at several sites, including

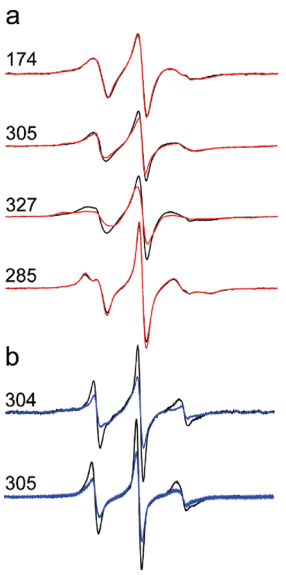

Figure 3. (a) Comparison of EPR spectra for several sites in syt1C2AB when bound to POPC/POPS bilayers with the addition of 1 (black) and 5 mol % PIP_2 (red). (b) EPR spectra in the absence of Ca^{2+} for two sites in syt1C2AB within the first Ca^{2+}-binding loop, C2B, when bound to either POPC/POPS (black) or POPC/POPS/PIP_2 (blue) bilayers. Spectra are normalized vs the total spin number and are 100 G scans.

the Ca^{2+}-binding loops of C2A as well as Ca^{2+}-binding loop 3 of C2B. These changes might reflect a different membrane association of syt1C2AB in the presence of PIP_2.

To determine whether changes in the EPR spectra reflect a difference in the association of syt1C2AB with the bilayer, each of the spectra in Figure 2 was power-saturated to obtain a measure of the depth of membrane penetration of each label (see Materials and Methods). The depth parameters obtained in the presence of PIP_2 are listed in Table 1, along with depth parameters obtained previously for syt1C2AB associated with POPC/POPS bilayers.[23] As one can see in Table 1, PIP_2 induces a deeper membrane penetration (more positive depth parameters) for sites in the Ca^{2+}-binding loops of C2A (173R1, 174R1, and 236R1), and PIP_2 alters the positions of labels within Ca^{2+}-binding loops of C2B (304R1, 305R1, 368R1, and 369R1). In addition, a site within the polybasic strand (327R1) moves closer to the membrane interface in the presence of PIP_2, and several sites opposite the Ca^{2+}-binding loops in C2B (396R1 and 285R1) reside at the membrane interface.

Increasing the PIP_2 Concentration Brings the Polybasic Face of C2B Closer to the Bilayer Interface. Levels of PIP_2 of up to 6 mol % have been detected at the focal sites of fusion, and we explored the effect of increasing the PIP_2 concentration from 1 to 5 mol %. In most cases, further increases in the level of PIP_2 do not significantly change line shapes (see Figure 3a) or depth parameters; however, EPR line shapes broaden for residues within the highly charged polybasic face of C2B, for example, at 327R1. For 327R1, increasing the PIP_2 concentration from 1 to 5 mol % increases the depth parameter, Φ, from −1.7 ± 0.1 to −1.1 ± 0.1, representing a shift in position toward the bilayer of approximately 3 Å. This is not unexpected. The incorporation of 5 mol % PIP_2 represents a significant increase in the membrane surface charge density, and increases in charge density are known to alter the equilibrium position of peptides that interact electrostatically with the membrane interface.[39]

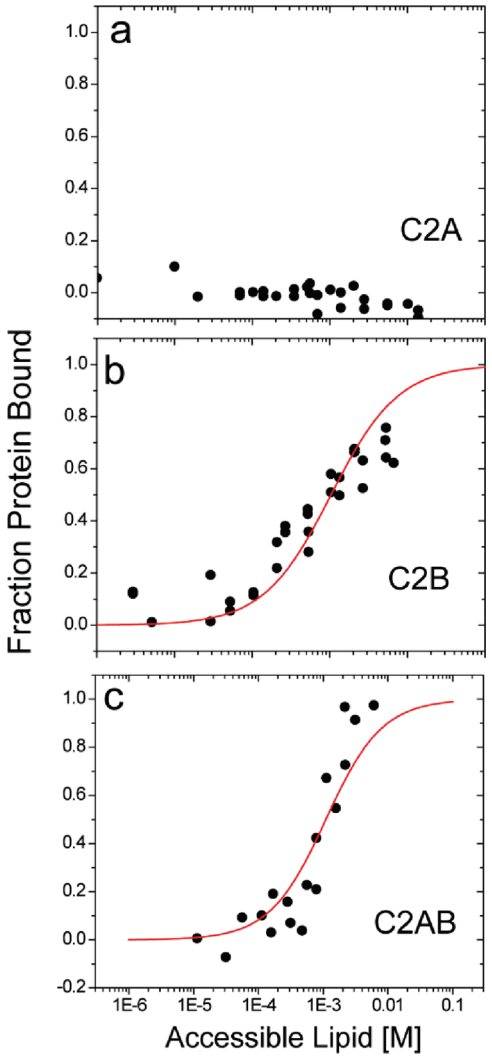

Figure 4. Ca^{2+}-independent partitioning of (a) C2A, (b) C2B, and (c) C2AB into POPC/POPS/PIP_2 (74:25:1) bilayers determined by sedimentation equilibrium. The red traces represent fits to the data using eq 3. No binding of C2A in the absence of Ca^{2+} to POPC/POPS/PIP_2 bilayers is detected. Reciprocal molar partition coefficients obtained from these data are listed in Table 3.

PIP_2 Enhances the Ca^{2+}-Independent Binding of syt1-C2AB. Previously, syt1C2AB was shown to interact with POPC/POPS bilayers in a Ca^{2+}-independent manner through the electrostatic association of the polybasic face of C2B with the bilayer interface.[13] Although this association is weak, the C2B domain will remain membrane-associated within the cell (if it is not associated with SNARE proteins) because it is tethered to the bilayer interface, thereby increasing the local lipid concentration. A well-established vesicle sedimentation assay was used to determine the partition coefficients for the C2A, C2B, and C2AB fragments of syt1 with the bilayer interface under conditions where the protein is dilute on the membrane interface. The binding data are shown in Figure 4 along with fits to the data using eq 3. There was no measurable affinity of the C2A domain for POPC/POPS/PIP_2 bilayers in the absence of Ca^{2+}. The reciprocal molar partition coefficients for C2B and C2AB obtained from the fits in Figure 4 are listed in Table 2. In the presence of PIP_2, syt1C2B and syt1C2AB have a similar bilayer affinity, and the domains will be half-membrane-bound at an accessible lipid concentration of approximately 1 mM. The values obtained previously in POPC/POPS bilayers are shown for comparison and indicate that addition of 1 mol % PIP_2 to POPC/POPS bilayers produces approximately 3- and 8-fold increases in membrane affinity for C2B and C2AB, respectively.

The incorporation of PIP_2 does not significantly change most EPR line shapes for membrane-associated syt1C2AB in the absence of Ca^{2+}, except within the first Ca^{2+}-binding loop of C2B (see Figure 3b). For these sites, membrane depth parameters indicate that the first Ca^{2+}-binding loop is positioned closer to the interface. For example, the depth parameter for 304R1 increases from -1.3 ± 0.1 without PIP_2 to -0.5 ± 0.4 with 1% PIP_2, indicating a shift into the interface of ~4 Å.

Table 2. Calcium-Independent Reciprocal Molar Partition Coefficients for syt1C2B and syt1C2AB with PC/PS (3:1) or PC/PS/PIP_2 (74:25:1) Membranes[a]

	C2A	C2B	C2AB
PC/PS/PIP_2	–	$(9.6 \pm 1.1) \times 10^2$	$(9.1 \pm 1.6) \times 10^2$
PC/PS	–	$(2.9 \pm 0.3) \times 10^2$	$(1.2 \pm 0.1) \times 10^2$

[a] Partition coefficients determined by sedimentation (see Materials and Methods) in the presence of 1 mM EGTA. Partition coefficients for PC/PS bilayers in the absence of Ca^{2+} are shown for comparison and were published previously.[13]

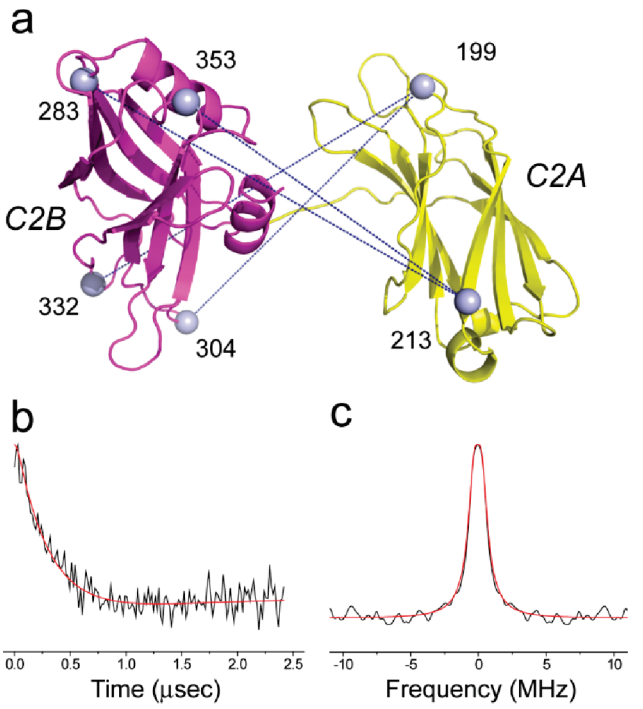

Figure 5. Pulse EPR (DEER) was used to measure distances between the C2A and C2B domains of syt1C2AB when bound to POPC/POPS/PIP_2 bilayers. Shown in panel a are sites for four spin-labeled pairs used for distance measurements. The black traces in panels b and c represent the background-subtracted DEER signal and Pake pattern obtained for the spin pair of 199R1 and 304R1, respectively. The red trace represents the fit to the data using a single Gaussian distribution, which is described by the mean distances and one standard deviation from the mean given in Table 3.

Table 3. Distances and Distance Distributions Obtained by Double Electron−Electron Resonance (DEER) between Spin-Labeled Sites in C2A and C2B[a]

C2A/C2B mutant	POPC/POPS (3:1)	POPC/POPS/PIP_2 (74:25:1)
R199R1/V304R1	40 ± 14 (Å)	39 ± 16 (Å)
R199R1/K332R1	46 ± 8	52 ± 11
K213R1/V283R1	61 ± 16	56 ± 12
K213R1/Q353R1	56 ± 15	53 ± 15

[a] Measurements were taken in the presence of Ca^{2+} (see Materials and Methods). Distances were obtained by a Gaussian fit to the distance distribution using DeerAnalysis2009.[47] The distances represent the most populated distances, and the range represents one standard deviation of the Gaussian distribution. The two shorter mutant pairs have an ∼2 Å distance uncertainty and a 30% uncertainty in the distribution. For the two distances of >50 Å, there is an ∼4 Å distance uncertainty and a 50% uncertainty in the distribution. Data for POPC/POPS bilayers were obtained previously[23] and are shown here for the sake of comparison.

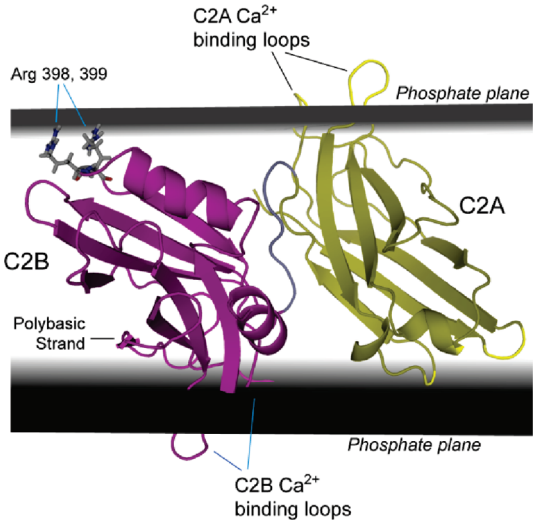

Figure 6. Model for the membrane-bound state of syt1C2AB when bound to POPC/POPS/PIP_2 (74:25:1) bilayers. The EPR-derived restraints could not be satisfied by docking to a single bilayer but require the calcium-binding loops of C2B (magenta) and C2A (yellow) to insert into opposing bilayers. A region close to two conserved arginine residues in C2B (residues 398 and 399), which are opposite the Ca^{2+}-binding loops, is located in the bilayer interface and requires that the C2B domain contact both membrane interfaces.

syt1C2AB Bridges Bilayers, and 1% PIP_2 Drives Bilayers Closer Together. The data listed in Table 1 provide point-to-plane depth restraints that may be used to assess the membrane docking of syt1C2AB. To provide additional structural restraints, we measured four distances across the two C2 domains of syt1 when fully bound to membranes containing PIP_2. Shown in Figure 5a are positions in syt1C2AB from which the interdomain restraints were measured. Also shown in Figure 5 are the background-corrected DEER signal and Pake pattern obtained for the nitroxide pair of 199R1 and 304R1. The signals obtained from 199R1 and 304R1 are similar to the three other signals, and they resemble those obtained previously in POPC/POPS bilayers.[23] These DEER signals result from a broad distance distribution between nitroxide pairs, and in this case, they reflect structural heterogeneity in the relative orientations of C2A and C2B. The distances obtained by pulse EPR are listed in Table 3, and they represent the most probable distance and one standard deviation of the width of the Gaussian used to fit the distance distribution. Each of the distances measured has a broad distribution and was similar to interdomain distances obtained for syt1C2AB bound to PC/PS bilayers.

Using the structural restraints listed in Tables 1 and 3, we generated a model for the membrane-bound form of syt1C2AB using an approach that was employed previously to dock syt1C2AB to PC/PS bilayers. Using these restraints, it was not possible to dock the two C2 domains of syt1 to a single bilayer (a result that was obtained previously using restraints generated in POPC/POPS bilayers[23]). However, the restraints could be satisfied by docking syt1C2AB to two bilayers, and the result is shown in Figure 6.

In the model shown in Figure 6, the first and third Ca^{2+}-binding loops of C2A and C2B penetrate into opposite bilayers. The polybasic face of C2B, which includes a number of basic residues along its fourth β-strand, is closely associated with one interface, and the region opposite the Ca^{2+}-binding loops of C2B also interacts with the bilayer interface. This interaction includes the pair of conserved residues, Arg-398 and Arg-399, that likely promote association with the POPC/POPS/PIP_2 bilayer.

In Figure 7, the model obtained here for syt1 bound to bilayers containing 1 mol % PIP_2 is compared with a model obtained previously in POPC/POPS bilayers.[23] In the presence of PIP_2, both domains penetrate more deeply into the bilayer through their Ca^{2+}-binding loops, with loop 3 of C2B penetrating ∼6 Å deeper in the presence of PIP_2. In addition, the polybasic face of C2B is drawn closer to the bilayer interface in the presence of PIP_2, which tilts the axis of C2B further from the bilayer normal. Because the C2B domain bridges bilayers and retains bilayer contact on two faces, the separation between bilayers that best satisfies the restraints in the presence of PIP_2 is shorter than that obtained without PIP_2. In the presence of PIP_2, the optimal separation between bilayers that produces structures with the lowest energy and with a minimal number of violations is approximately 35 Å, whereas in the absence of PIP_2, the optimal separation was approximately 43 Å. On the basis of the error in the depth measurements and the variation in structures obtained from the simulated annealing, we estimate that the 8 Å decrease in distance has an error of approximately ±3 Å.

It should be noted that the structures shown in Figures 6 and 7 represent the lowest-energy structures obtained from a set of structures obtained by simulated annealing. Caution needs to be taken when interpreting any one structure, as there is considerable variability in the structures obtained (the root-mean-square deviation of the 10 lowest-energy structures obtained in the presence of 1 mol % PIP_2 was 3.77 ± 1.25 Å). Nonetheless, the results indicate that PIP_2, mediated by electrostatic interactions with syt1C2AB, acts to bring two opposing bilayers closer together.

DISCUSSION

At present, the role of PIP_2 in membrane fusion is not understood. PIP_2 is known to play an important role in cell signaling, functioning as a precursor to cellular second messengers and acting as a signaling lipid itself. At a molecular level, PIP_2 frequently acts to bind and translocate proteins containing specific domains, such as PH domains, to the membrane

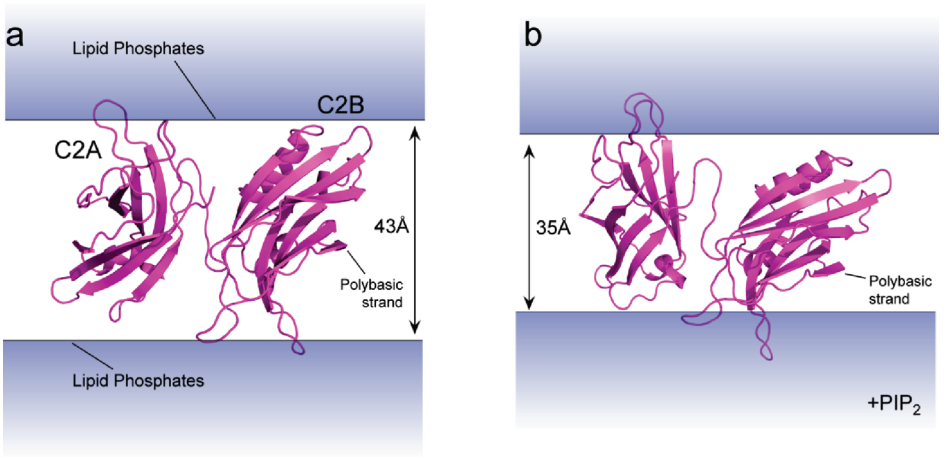

Figure 7. Comparison of the models for membrane-bound syt1C2AB when associated with membrane vesicles composed of (a) POPC and POPS (3:1) or (b) POPC, POPS, and PIP_2 (74:25:1). The addition of 1 mol % PIP_2 results in a model in which the calcium binding loops of C2A and C2B are more deeply inserted, the polybasic strand of C2B is closer to the membrane interface, and the bilayer spacing that best fits the EPR-derived restraints is 5−8 Å shorter than that for POPC/POPS bilayers.

surface,[40] and it is known to facilitate the attachment of positively charged segments of proteins to the membrane interface through electrostatic interactions.[41] Moreover, basic protein motifs have the capacity to sequester PIP_2, thereby regulating the lateral distribution and activity of PIP_2 within the bilayer. Indeed, there is evidence that the highly charged juxtamembrane region of syntaxin interacts with PIP_2 and controls the activity of this lipid within the focal site of fusion.[29] Because PIP_2 has a highly positive intrinsic curvature, it should be highly inhibitory to fusion when present on the cytoplasmically facing target monolayer. As a result, it has been suggested that PIP_2 might act to prevent fusion until it is removed during the final triggering step for exocytosis. There is also evidence that PIP_2 plays a direct role in fusion by helping bridge bilayers through electrostatic interactions with the positively charged juxtamembrane segment of the vesicle SNARE synaptobrevin.[42]

In this work, we utilized both pulse and continuous wave EPR spectroscopy to generate a model for syt1C2AB when bound to POPC/POPS bilayers containing 1 mol % PIP_2. The model suggests that PIP_2 modulates the configuration of syt1 and may act to decrease the spacing between bilayers at the focal site of fusion. In this model, the Ca^{2+}-binding loops of the C2 domains of syt1 penetrate more deeply into bilayers in the presence of PIP_2 and the orientation of the C2B domain changes to bring the polybasic face of this domain closer to the membrane interface. The restraints obtained here indicate that the C2B domain of syt1 must bridge bilayers, and the results of simulated annealing indicate that the most likely configurations are those in which the C2A and C2B domains bind opposing bilayers. Because the C2B domain bridges bilayers, the change in orientation of C2B results in a shorter distance between the two opposing bilayers.

The model shown in Figures 6 and 7b was obtained for syt1C2AB bound to bilayers that both contain 1 mol % PIP_2. In the cell, the majority of the PIP_2 is believed to be present on the plasma membrane interface and not the vesicle interface,[29] and unlike this experimental system, the native system is not symmetric. Although we have no data for an asymmetric system, the two C2 domains have different Ca^{2+}-dependent lipid preferences, with the C2B domain preferring to associate with PIP_2-containing bilayers and the C2A domain preferring PS-containing bilayers.[8] As a result, the calcium binding loops of C2A and C2B would be predicted to associate with the vesicle and plasma membranes, respectively. The presence of PIP_2 in the target membrane is expected to have an effect similar to that seen in our model system. The presence of PIP_2 on the plasma membrane surface should enhance interactions with the polybasic face of C2B, alter the C2B domain orientation, and decrease bilayer separation.

The C2B domain is a highly charged protein domain, and electrostatic surface potential plots (showing the 25 and −25 mV equipotential surfaces) for the C2B domain in Ca^{2+}-free and Ca^{2+}-bound forms are shown in Figure 8. The addition of Ca^{2+} creates a region of positive electrostatic potential around the Ca^{2+}-binding loops of C2B, and the polarization of this region likely triggers insertion of the C2B domain into lipid bilayers in a manner similar to that for the C2A domain.[24] Even in the absence of Ca^{2+}, the C2B domain is highly positively charged, with regions of large positive surface potential near the polybasic face and the region opposite the Ca^{2+}-binding loops. These electrostatic features likely mediate the change in orientation of the C2B domain in the presence of PIP_2 and the membrane contact that is observed in a region opposite the Ca^{2+}-binding loops (see Figure 6).[23] Two conserved basic residues opposite the Ca^{2+}-binding loops of on C2B, Arg-398 and Arg-399 (Figures 6 and 8), make a significant contribution to the positive electrostatic potential on this end of the domain, and they are also functionally important. When these residues are mutated to glutamine, Ca^{2+}-trigged synchronous release is nearly abolished.[25]

The model shown in Figure 6 seems physically plausible. The two opposing bilayers are both negatively charged; however, strong electrostatic repulsion should not take place because the separation between bilayers is greater than twice the Debye length at normal ionic strength. As indicated above, the C2B domain is highly positively charged, and as a result, syt1 acts as an electrostatic mediator to bring the two bilayers closer together. The changes seen here in C2 domain orientation upon addition of PIP_2 are not unexpected, because previous work provided qualitative evidence of changes in C2B domain orientation in the presence of PIP_2.[8,12] PIP_2 has been observed to modulate the binding and orientation of the C2 domain of PKCα;[43] however, in this case, the domain is tilted toward the bilayer normal in the

dx.doi.org/10.1021/bi200049c |*Biochemistry* 2011, 50, 2633–2641

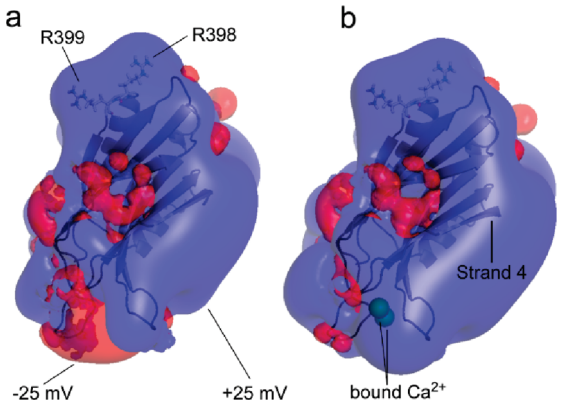

Figure 8. Equipotential electrostatic surfaces [25 mV (blue) and −25 mV (red)] for (a) the C2B domain in the absence of Ca^{2+} and (b) the C2B domain in the presence of Ca^{2+}. The C2B domain is highly positively charged and has regions of positive charge because of its polybasic strand (strand 4) and highly conserved arginine residues located on a surface opposite the Ca^{2+}-binding loops. The binding of Ca^{2+} polarizes the primary membrane-binding face of the domain. The potentials were calculated using the APBS plug-in from PyMOL.

presence of PIP_2. The different behavior of the syt1 and PKC domains appears to be due to differences in the PIP_2-interacting face of these domains. Unlike the syt1 C2B domain, which likely responds to PIP_2 through a purely electrostatic mechanism, the behavior of the PKCα C2 domain appears to be due to a specific binding site for the PIP_2 headgroup on the domain.[44]

Evidence of bilayer bridging by syt1C2AB has been observed previously, and it could play an important role in syt1 function. As indicated above, a model generated previously in POPC/POPS bilayers (using 21 point-to-plane and 12 interdomain distance restraints) places syt1C2AB in a configuration to bridge bilayers (Figure 7a). Moreover, light scattering and electron microscopy both indicate that syt1C2AB aggregates vesicles in a Ca^{2+}-dependent fashion.[21,22] Evidence of bilayer bridging also comes from functional assays of syt1 function. Recently, fusion in a Ca^{2+}-dependent manner mediated by syt1 has been demonstrated using full-length syt1 and a single-vesicle fusion assay.[45] In this case, high PIP_2 levels were required in the target membrane for optimal Ca^{2+} sensitivity, suggesting that a transbilayer interaction of syt1 was required to stimulate fusion. This work is consistent with earlier work in a bulk vesicle fusion assay, indicating that transbilayer interactions of syt1 were likely to mediate fusion.[46]

In summary, our work indicates that PIP_2, by changing the membrane position and orientation of syt1, acts to drive vesicle and target membranes closer together. How might membrane bridging or transbilayer interactions of syt1 mediate synchronous Ca^{2+}-dependent neurotransmitter release? Conceivably, this bridging activity might act to trigger the assembly and zippering of the SNARE complex from either a disassembled or partially assembled state. Bilayer bridging might also act to promote the mixing of lipids in the two opposing bilayers and the formation of a fusion stalk. It has been proposed that syt1 acts by altering lipid order or curvature strain,[19] thereby promoting the formation of a fusion stalk. Conceivably, the deeper penetration of the C2 domains and the presence of PIP_2, which may be sequestered near the focal site of fusion, could act to amplify the local positive membrane curvature strain near the site of fusion.

AUTHOR INFORMATION

Corresponding Author

*Department of Chemistry, University of Virginia, McCormick Road, Charlottesville, VA 22904-4319. E-mail: cafiso@virginia.edu. Telephone: (434) 924-3067. Fax: (434) 924-3567.

Funding Sources

This work was supported by Grant GM 072694 from the National Institute of General Medical Sciences, National Institutes of Health.

ACKNOWLEDGMENT

We thank Christian Altenbach (University of California, Los Angeles, CA) for providing LabVIEW, used to process and simulate EPR spectra. We also acknowledge helpful discussions with Jeff Ellena and Lukas Tamm (University of Virginia) and Reinhard Jahn (Max-Plank-Institute Göttingen, Göttingen, Germany).

ABBREVIATIONS

DEER, double electron−electron resonance; EPR, electron paramagnetic resonance; MTSL, methanethiosulfonate spin-label; PIP_2 or $PI(4,5)P_2$, phosphatidylinositol 4,5-bisphosphate; PC, phosphatidylcholine; POPC, palmitoyloleoylphosphatidylcholine; POPS, palmitoyloleoylphosphatidylserine; PS, phosphatidylserine; R1, spin-labeled side chain produced by derivatization of a cysteine with the MTSL; SDSL, site-directed spin labeling; SNARE, soluble *N*-ethylmaleimide-sensitive factor attachment protein receptor; syt1, synaptotagmin 1; syt1C2AB, soluble fragment of syt1 containing the tandem C2A and C2B domains.

REFERENCES

(1) Sudhof, T. C. (2004) The synaptic vesicle cycle. *Annu. Rev. Neurosci. 27*, 509–547.

(2) Chapman, E. R. (2008) How does synaptotagmin trigger neurotransmitter release? *Annu. Rev. Biochem. 77*, 615–641.

(3) Rothman, J. E. (1994) Intracellular membrane fusion. *Adv. Second Messenger Phosphoprotein Res. 29*, 81–96.

(4) Rizo, J., Chen, X., and Arac, D. (2006) Unraveling the mechanisms of synaptotagmin and SNARE function in neurotransmitter release. *Trends Cell Biol. 16*, 339–350.

(5) Jahn, R., and Scheller, R. H. (2006) SNAREs: Engines for membrane fusion. *Nat. Rev. 7*, 631–643.

(6) James, D. J., Kowalchyk, J., Daily, N., Petrie, M., and Martin, T. F. (2009) CAPS drives trans-SNARE complex formation and membrane fusion through syntaxin interactions. *Proc. Natl. Acad. Sci. U.S.A. 106*, 17308–17313.

(7) Rizo, J., and Rosenmund, C. (2008) Synaptic vesicle fusion. *Nat. Struct. Mol. Biol. 15*, 665–674.

(8) Bai, J., Tucker, W. C., and Chapman, E. R. (2004) PIP2 increases the speed of response of synaptotagmin and steers its membrane-penetration activity toward the plasma membrane. *Nat. Struct. Mol. Biol. 11*, 36–44.

(9) Bai, J., and Chapman, E. R. (2004) The C2 domains of synaptotagmin: Partners in exocytosis. *Trends Biochem. Sci. 29*, 143–151.

(10) Frazier, A. A., Roller, C. R., Havelka, J. J., Hinderliter, A., and Cafiso, D. S. (2003) Membrane-bound orientation and position of the synaptotagmin I C2A domain by site-directed spin labeling. *Biochemistry 42*, 96–105.

(11) Herrick, D. Z., Sterbling, S., Rasch, K. A., Hinderliter, A., and Cafiso, D. S. (2006) Position of synaptotagmin I at the membrane interface: Cooperative interactions of tandem C2 domains. *Biochemistry 45*, 9668–9674.

(12) Rufener, E., Frazier, A. A., Wieser, C. M., Hinderliter, A., and Cafiso, D. S. (2005) Membrane-bound orientation and position of the synaptotagmin C2B domain determined by site-directed spin labeling. *Biochemistry 44*, 18–28.

(13) Kuo, W., Herrick, D. Z., Ellena, J. F., and Cafiso, D. S. (2009) The calcium-dependent and calcium-independent membrane binding of synaptotagmin 1: Two modes of C2B binding. *J. Mol. Biol. 387*, 284–294.

(14) Brunger, A. T. (2005) Structure and function of SNARE and SNARE-interacting proteins. *Q. Rev. Biophys. 38*, 1–47.

(15) Dai, H., Shen, N., Arac, D., and Rizo, J. (2007) A quaternary SNARE-synaptotagmin-Ca^{2+}-phospholipid complex in neurotransmitter release. *J. Mol. Biol. 367*, 848–863.

(16) Choi, U. B., Strop, P., Vrljic, M., Chu, S., Brunger, A. T., and Weninger, K. R. (2010) Single-molecule FRET-derived model of the synaptotagmin 1-SNARE fusion complex. *Nat. Struct. Mol. Biol. 17*, 318–324.

(17) Lai, A. L., Huang, H., Herrick, D. Z., Epp, N., and Cafiso, D. S. (2011) Synaptotagmin 1 and SNAREs Form a Complex That Is Structurally Heterogeneous. *J. Mol. Biol. 405*, 696–706.

(18) Martens, S., Kozlov, M. M., and McMahon, H. T. (2007) How synaptotagmin promotes membrane fusion. *Science 316*, 1205–1208.

(19) McMahon, H. T., Kozlov, M. M., and Martens, S. (2010) Membrane curvature in synaptic vesicle fusion and beyond. *Cell 140*, 601–605.

(20) Sorensen, J. B. (2009) Conflicting views on the membrane fusion machinery and the fusion pore. *Annu. Rev. Cell Dev. Biol. 25*, 513–537.

(21) Arac, D., Chen, X., Khant, H. A., Ubach, J., Ludtke, S. J., Kikkawa, M., Johnson, A. E., Chiu, W., Sudhof, T. C., and Rizo, J. (2006) Close membrane-membrane proximity induced by Ca^{2+}-dependent multivalent binding of synaptotagmin-1 to phospholipids. *Nat. Struct. Mol. Biol. 13*, 209–217.

(22) Connell, E., Giniatullina, A., Lai-Kee-Him, J., Tavare, R., Ferrari, E., Roseman, A., Cojoc, D., Brisson, A. R., and Davletov, B. (2008) Cross-linking of phospholipid membranes is a conserved property of calcium-sensitive synaptotagmins. *J. Mol. Biol. 380*, 42–50.

(23) Herrick, D. Z., Kuo, W., Huang, H., Schwieters, C. D., Ellena, J. F., and Cafiso, D. S. (2009) Solution and membrane-bound conformations of the tandem C2A and C2B domains of synaptotagmin 1: Evidence for bilayer bridging. *J. Mol. Biol. 390*, 913–923.

(24) Murray, D., and Honig, B. (2002) Electrostatic control of the membrane targeting of C2 domains. *Mol. Cell 9*, 145–154.

(25) Xue, M., Ma, C., Craig, T. K., Rosenmund, C., and Rizo, J. (2008) The Janus-faced nature of the C(2)B domain is fundamental for synaptotagmin-1 function. *Nat. Struct. Mol. Biol. 15*, 1160–1168.

(26) Martin, T. F. (1997) Stages of regulated exocytosis. *Trends Cell Biol. 7*, 271–276.

(27) Martin, T. F. (2001) $PI(4,5)P_2$ regulation of surface membrane traffic. *Curr. Opin. Cell Biol. 13*, 493–499.

(28) Takamori, S., Holt, M., Stenius, K., Lemke, E. A., Gronborg, M., Riedel, D., Urlaub, H., Schenck, S., Brugger, B., Ringler, P., Muller, S. A., Rammner, B., Grater, F., Hub, J. S., De Groot, B. L., Mieskes, G., Moriyama, Y., Klingauf, J., Grubmuller, H., Heuser, J., Wieland, F., and Jahn, R. (2006) Molecular anatomy of a trafficking organelle. *Cell 127*, 831–846.

(29) James, D. J., Khodthong, C., Kowalchyk, J. A., and Martin, T. F. (2008) Phosphatidylinositol 4,5-bisphosphate regulates SNARE-dependent membrane fusion. *J. Cell Biol. 182*, 355–366.

(30) McLaughlin, S., and Murray, D. (2005) Plasma membrane phosphoinositide organization by protein electrostatics. *Nature 438*, 605–611.

(31) Sambrook, J., Fritsch, E. F., and Maniatis, T. (1989) *Molecular Cloning: A Laboratory Manual*, Cold Spring Harbor Laboratory Press, Plainview, NY.

(32) Wang, J., Gambhir, A., Hangyas-Mihalyne, G., Murray, D., Golebiewska, U., and McLaughlin, S. (2002) Lateral sequestration of phosphatidylinositol 4,5-bisphosphate by the basic effector domain of myristoylated alanine-rich C kinase substrate is due to nonspecific electrostatic interactions. *J. Biol. Chem. 277*, 34401–34412.

(33) Frazier, A. A., Wisner, M. A., Malmberg, N. J., Victor, K. G., Fanucci, G. E., Nalefski, E. A., Falke, J. J., and Cafiso, D. S. (2002) Membrane orientation and position of the C2 domain from cPLA2 by site-directed spin labeling. *Biochemistry 41*, 6282–6292.

(34) Buser, C. A., and McLaughlin, S. (1998) Ultracentrifugation technique for measuring the binding of peptides and proteins to sucrose-loaded phospholipid vesicles. *Methods Mol. Biol. 84*, 267–281.

(35) Ames, B. N. (1966) Assay of inorganic phosphate, total phosphate and phosphatases. In *Methods in Enzymology* (Neufeld, E. F., and Ginsburg, V., Eds.) pp 115−118, Academic Press, San Diego.

(36) Baker, N. A., Sept, D., Joseph, S., Holst, M. J., and McCammon, J. A. (2001) Electrostatics of nanosystems: Application to microtubules and the ribosome. *Proc. Natl. Acad. Sci. U.S.A. 98*, 10037–10041.

(37) Fernandez, I., Araç, D., Ubach, J., Gerber, S. H., Shin, O.-h., Gao, Y., Anderson, R. G. W., Südhof, T. C., and Rizo, J. (2001) Three-Dimensional Structure of the Synaptotagmin 1 C2B-Domain: Synaptotagmin 1 as a Phospholipid Binding Machine. *Neuron 32*, 1057–1069.

(38) Falke, J. J., Drake, S. K., Hazard, A. L., and Peersen, O. B. (1994) Molecular Tuning of Ion Binding to Calcium Signaling Proteins. *Q. Rev. Biophys. 27*, 219–290.

(39) Qin, Z., and Cafiso, D. S. (1996) Membrane structure of protein kinase C and calmodulin binding domain of myristoylated alanine rich C kinase substrate determined by site-directed spin labeling. *Biochemistry 35*, 2917–2925.

(40) Overduin, M., Cheever, M. L., and Kutateladze, T. G. (2001) Signaling with phosphoinositides: Better than binary. *Mol. Interventions 1*, 150–159.

(41) McLaughlin, S., Wang, J., Gambhir, A., and Murray, D. (2002) PIP_2 and proteins: Interactions, organization, and information flow. *Annu. Rev. Biophys. Biomol. Struct. 31*, 151–175.

(42) Williams, D., Vicogne, J., Zaitseva, I., McLaughlin, S., and Pessin, J. E. (2009) Evidence that electrostatic interactions between vesicle-associated membrane protein 2 and acidic phospholipids may modulate the fusion of transport vesicles with the plasma membrane. *Mol. Biol. Cell 20*, 4910–4919.

(43) Landgraf, K. E., Malmberg, N. J., and Falke, J. J. (2008) Effect of PIP2 binding on the membrane docking geometry of PKC α C2 domain: An EPR site-directed spin-labeling and relaxation study. *Biochemistry 47*, 8301–8316.

(44) Guerrero-Valero, M., Ferrer-Orta, C., Querol-Audi, J., Marin-Vicente, C., Fita, I., Gomez-Fernandez, J. C., Verdaguer, N., and Corbalan-Garcia, S. (2009) Structural and mechanistic insights into the association of PKCα-C2 domain to $PtdIns(4,5)P_2$. *Proc. Natl. Acad. Sci. U.S.A. 106*, 6603–6607.

(45) Lee, H. K., Yang, Y., Su, Z., Hyeon, C., Lee, T. S., Lee, H. W., Kweon, D. H., Shin, Y. K., and Yoon, T. Y. (2010) Dynamic Ca^{2+}-dependent stimulation of vesicle fusion by membrane-anchored synaptotagmin 1. *Science 328*, 760–763.

(46) Stein, A., Radhakrishnan, A., Riedel, D., Fasshauer, D., and Jahn, R. (2007) Synaptotagmin activates membrane fusion through a Ca^{2+}-dependent trans interaction with phospholipids. *Nat. Struct. Mol. Biol. 14*, 904–911.

(47) Jeschke, G., Chechik, V., Ionita, P., Godt, A., Zimmermann, H., Banham, J., Timmel, C., Hilger, D., and Jung, H. (2006) DeerAnalysis2006: A comprehensive software package for analyzing pulsed ELDOR data. *Appl. Magn. Reson. 30*, 473–498.